Applied Catalysis B: Environmental 176–177 (2015) 130–138

Contents lists available at ScienceDirect

Applied Catalysis B: Environmental

journal homepage: www.elsevier.com/locate/apcatb

Comprehensive study of H_2S selective catalytic oxidation on combined oxides derived from Mg/Al-$V_{10}O_{28}$ layered double hydroxides

Xin Zhang [a], Yuyin Tang [a], Nanli Qiao [a], Yang Li [a], Siqiu Qu [b], Zhengping Hao [a,*]

[a] Department of Environmental Nano-materials, Research Center for Eco-Environmental Sciences, Chinese Academy of Sciences, Beijing 100085, PR China
[b] Center of Research & Development, Shandong Sunway Petrochemical Engineering Share Co., Ltd., Beijing 100015, PR China

ARTICLE INFO

Article history:
Received 20 December 2014
Received in revised form 27 March 2015
Accepted 31 March 2015
Available online 1 April 2015

Keywords:
Layered double hydroxides
Derived oxides
H_2S selective oxidation
Catalytic activity
Catalytic mechanism

ABSTRACT

A series of Mg_2Al-$V_{10}O_{28}$-LDH (named V-LDH) were synthesized using ion-exchange method, and the derived oxides were investigated for H_2S selective oxidation. The physicochemical properties of the catalysts were assessed by various methods. It was observed that vanadium species existed mainly in the form of isolated V^{5+} in distorted [VO_4], $Mg_3V_2O_8$, and $Mg_2V_2O_7$. Moreover, there was a large amount of V^{4+} species (>25%), mainly formed with vanadyl bonds. Significantly, the catalysts exhibited excellent catalytic performances at relatively low reaction temperatures (100–200 °C). Furthermore, the catalyst containing 10.6 wt% vanadium (8V-LDO) was highly durable at a relatively low temperature (160 °C) and a high gas hourly space velocity (GHSV, 24,000 h^{-1}), which can proceed consecutively for 100 h without notable deactivation. In the reaction process, the gradually produced sulfate species reacted with V^{4+} species to form less active $VOSO_4$ species, which improved the redox property of V^{5+}. The catalysts obeyed a step-wise mechanism for H_2S selective catalytic oxidation. The excellent durability can be ascribed to the fact that the content of moderate basic sites was kept and the redox property of V^{5+} was improved.

1. Introduction

H_2S is one of the most toxic air pollutants and mainly originates from several branches of the chemical industry. Today, H_2S is usually removed by the well-known Claus process [1,2]. However, it is still difficult to reach a permissible level of sulfur emissions due to the thermodynamic limitations of the Claus process and increasingly stringent environmental regulations. Fortunately, the remaining H_2S in Claus tail gas, almost 1%, can be eliminated to a great extent by various additional purification processes [3]. From a practical point of view, selective catalytic oxidation techniques have been of great research interest in past decades, because it possible to directly catalytically oxidize H_2S to elemental sulfur. The irreversible reaction equations are as follows: Eq. (1) as the main reaction; Eqs. (2) and (3) as side reactions [4].

$$H_2S + 1/2O_2 \rightarrow (1/n)S_n + H_2O \quad (1)$$

$$1/nS_n + O_2 \rightarrow SO_2 \quad (2)$$

$$H_2S + 3/2O_2 \rightarrow SO_2 + H_2O \quad (3)$$

However, a major technical challenge associated with achieving selective oxidation of H_2S is the formation of other undesirable sulfur species. For example, SO_2 can be formed in the reaction by the deep oxidation of H_2S or the further oxidation of elemental sulfur, causing a decrease in sulfur yield. Thus, the efficient removal of sulfur in selective oxidation processes depends strongly on the development of new active and selective catalysts.

Vanadium oxides have been reported to be active and selective for H_2S selective oxidation in the 200–300 °C temperature range. Many supported vanadium oxide catalysts, such as V_2O_5 supported on pillared clay alumina [3,5,6], and titania have been investigated intensively as potential catalysts. The characteristics of the support and dispersion of the vanadium species strongly influence the catalytic performance of such supported vanadium catalysts. However, the choice of an optimal support is a complex problem [7], because the support can react with H_2S or reaction products to form sulfate, causing a decrease in the desired catalytic activity or even destruction of the catalyst. In addition, the dispersion and particle size of the vanadium species cannot be tuned readily. Furthermore, catalyst deactivation should be seriously considered for supported vanadium catalysts for their use in industrial emission control. Moreover, the reaction temperature for supported vanadium catalysts is too high in terms of energy requirements. Thus, there is a continuing need to modify present vanadium species to

* Corresponding author. Tel.: +86 10 62923564; fax: +86 10 62923564.
E-mail address: zpinghao@rcees.ac.cn (Z. Hao).

http://dx.doi.org/10.1016/j.apcatb.2015.03.057
0926-3373/

develop a catalyst with higher catalytic performance, outstanding stability, and one that operates at lower reactions temperatures.

Layered double hydroxides (LDHs), also known as hydrotalcite-like compounds, are anionic clay materials [8]. The chemical composition of LDHs can be expressed by the general formula $[M^{II}_{1-x}\ M^{III}_{x}(OH)_2]^{x+}\ [A_{x/n}{}^{n-}{\cdot}yH_2O]^{x-}$ [9], where M^{II} and M^{III} are divalent and trivalent metal cations [10], A^{n-} is a n-valent anion, and x usually has values between 0.25 and 0.33, is used to balance the positive charge in the brucite like layer. The interlayer anion can be exchanged readily, and the interlayer spacing can be modified markedly depending on the precise nature, size, geometry, and orientation of the interlayer anions. In particular, LDHs and their derivatives have been intensively investigated in recent years as catalysts and catalyst supports for many reactions. Because the acid/base properties can be tuned readily [11] and the composition can be varied [10], this creates great flexibility for the selection of various cations in these materials for H_2S selective oxidation. The corresponding composite oxides can be obtained after calcination, where the metal oxides are well-mixed and highly dispersed. Thus, layered double hydroxides are considered an attractive and suitable material to disperse and modify vanadium species.

In our previous work [12], vanadium species were introduced into the brucite-like layer of LDHs by partial replacement of Al. The corresponding mixed oxides were tested for H_2S selective catalytic oxidation. The mixed oxides exhibited high catalytic activities at relatively lower temperatures and high gas hourly space velocity (GHSV). However, further application was limited by poor stability, which decreased markedly after 20 h of reaction. Thus, in this paper, vanadium species were incorporated into the LDH interlayer in the form of decavanadate by anion exchange, i.e., Mg_2Al-$V_{10}O_{28}$-LDH (named V-LDH) [13]. The preparation process includes synthesis of LDH and the anion exchange step, providing a facile method to obtain Mg_2Al-LDH, which was further used to synthesize the Mg_2Al-$V_{10}O_{28}$-LDH precursor. The derived oxides containing vanadium (V-LDO) were obtained after calcination and used for H_2S selective catalytic oxidation. Moreover, the physicochemical properties of catalysts were also determined using various characterization techniques to better understand the catalytic and catalyst deactivation mechanisms.

2. Experimental

2.1. Catalyst preparation

The synthesis of Mg_2Al-LDH was carried out using a modified version of Xu's method [14]. $MgNO_3$, $Al(NO_3)_3$ and NaOH were used as starting materials. In a typical synthesis process, 60 mmol $Mg(NO_3)_2$, 30 mmol $Al(NO_3)_3$ were dissolved in 200 ml decarbonated water previously purged by nitrogen. Then, the solution was quickly added into 800 ml of NaOH solution (0.15 M) under vigorous stirring, followed by 15 min stirring in nitrogen atmosphere. Mg_2Al-NO_3-LDH was obtained after centrifuge 3 times and dried overnight at 40 °C.

The anion exchange was proceeded by referring Dula's method [15]. A portion of 3 g of Mg_2Al-NO_3-LDH was suspended in 75 ml decarbonated water previously purged by nitrogen. This suspension was stirred at 55 °C and under nitrogen flow for 1 h, and then a solution of $NaVO_3$ containing 5, 8, 10 and 20 wt% vanadium dissolved in 150 ml decarbonated water was dropwised added, respectively. The mixture was maintained at 55 °C in nitrogen atmosphere for 1 h. During the exchange period, the pH was dropped and maintained constant at 4.5 by adjusting with HNO_3 0.1 M (vanadium mainly exists in the form of $V_{10}O_{28}{}^{6-}$). The resulting products were filtered, washed thoroughly with deionized and decarbonated water and dried overnight at 40 °C. These LDH materials (Mg_2Al-$V_{10}O_{28}$-LDH) were denoted as 5V-LDH, 8V-LDH, 10V-LDH and 20V-LDH. Finally, the derived oxides catalysts were obtained after calcining the LDH materials at 550 °C for 4 h. These catalysts were denoted as 5V-LDO, 8V-LDO, 10V-LDO and 20V-LDO.

2.2. Characterization of the catalysts

X-ray diffraction (XRD) patterns were recorded on a PANalytical X'Pert PRO powder diffraction system using Cu K radiation(λ = 0.15418 nm) in the 2θ range of 10–80° (scanning rate of 0.5°/min).

Fourier transform infrared (FT-IR) spectroscopy was measured by the KBr method recorded on a Bruker Tensor 27, scanned from 4000 to 600 cm^{-1}.

Thermal stability was investigated with thermogravimetry (TG, Seteram, Labsys). Typically, around 30 mg of sample was heated in an Al_2O_3 crucible at a constant heating rate of 10 °C/min from 25 to 1000 °C, with air purging at a flow rate of 30 ml/min.

X-ray photoelectron spectra (XPS) were recorded with a Thermo Electron Escalab250 instrument using Al Kα radiation. The binding energies were calibrated using C1 s peak of contaminant carbon (BE = 285 eV) as standard, and quoted with a precision of ±0.2 eV.

BET surface areas and textural properties of catalysts were determined by nitrogen adsorption–desorption isotherms using a gas sorption analyzer NOVA1200. Prior to N_2 adsorption measurement, the samples were degassed at 300 °C for 3 h.

The electron paramagnetic resonance (EPR) spectra were recorded on a JES FA200 spectrometer at room temperature.

H_2 temperature-programmed reduction (H_2-TPR) experiments were conducted on a Micromeritics Chemisorb 2720 apparatus. TPR profiles were obtained by passing a 5% H_2/He flow (50 ml/min) through the pretreated catalyst (about 100 mg). Temperature was increased from room temperature to 900 °C at a rate of 10 °C/min. Hydrogen concentration in the effluent was continuously monitored by a thermo conductivity detector. Prior to each TPR run, catalyst was pre-heated in He flow from room temperature to 300 °C and held for 30 min.

CO_2 temperature-programmed desorption (CO_2-TPD) was carried out on the same apparatus as that in H_2-TPR. In the process, the sample was heated from room temperature to 900 °C at a rate of 10 °C/min in pure He. Before each TPD test, 100 mg sample was pre-heated in He flow from room temperature to 300 °C and held for 30 min. After cooling to room temperature, 20% CO_2/He was fed to the reactor at 50 ml/min for 30 min, then, pure He was fed to the reactor at 50 ml/min for 30 min to purge away any residual CO_2.

The chemical analysis was carried out by inductively coupled plasma optical emission spectrometer (ICP-OES, Prodigy, Leeman, USA).

2.3. Catalytic performance tests

All tests were performed in a continuous flow fixed-bed quartz reactor at atmospheric pressure. A 0.5 ml catalyst (20–40 mesh, size of 0.38–0.83 mm) was placed in the central section of the reactor. The mixture gas containing 5000 ppm H_2S, 2500 ppm O_2 and balance gas (N_2) were fed into the reactor at 200 ml/min of the total gas flow rate (GHSV = 24,000 h^{-1}) and reacted in temperature range of 100–200 °C. After reaction, the effluent stream was detected by a gas chromatograph (GC126) equipped with a FPD and a TCD. A condenser was located at the bottom of the reactor to trap the sulfur gas in effluent stream. Instantaneous fractional conversion of H_2S, sulfur selectivity and sulfur yield were defined as:

$$H_2S\ \text{conversion} = \frac{(H_2S)_{in} - (H_2S)_{\text{out}}}{(H_2S)_{\text{in}}}$$

$$\text{Sulfurselectivity} = \frac{(H_2S)_{in} - (H_2S)_{out} - (SO_2)_{out}}{(H_2S)_{in} - (H_2S)_{out}}$$

$$\text{Sulfuryield} = H_2S\text{conversion} \times \text{Sulfurselectivity}$$

3. Results and discussion

3.1. Characterization of Mg_2Al-$V_{10}O_{28}$-LDHs

The XRD patterns of the vanadium-containing parent LDH materials are shown in Fig. 1. It can be seen that all samples are dominated by peaks appearing at about 10°, 20°, 35°, 39°, 45°, 60°, and 61°, attributable to the (0 0 3), (0 0 6), (0 1 2), (0 1 5), (0 1 8), (1 1 0), and (1 1 3) planes, respectively, which are typical of diffraction patterns of LDH materials [16]. Moreover, a shoulder peak at 12° related to carbonate species was observed for Mg_2Al-LDH, which can be attributed to that little carbonate species was exchanged into the material in the preparation process. Furthermore, the diffraction intensity decreases gradually with the rise in vanadium content, compared to Mg_2Al-LDH. It is known that the brucite-like layer and anion interlayer contribute together to the diffraction intensity of the planes. However, the LDH materials in this study have the same brucite-like layer. Thus, the observed gradually lower diffraction intensities resulted from the higher atomic scattering factor with the rise in vanadium content in the interlayer [17,18]. Thus, it indicates that vanadium species were incorporated successfully into the LDH interlayers. Moreover, the (1 1 0) plane can be used to determine the lattice parameter *a*, corresponding to the average cation–cation distance in a brucite layer. The (0 0 3) and (0 0 6) planes can be used to calculate parameter *c*, which is related to the total thickness of the brucite-like layer and the interlayer distance [19,20]. The lattice parameter *a* is 3.04 for all samples, which indicates that the original structure of the brucite-like layer is intact. However, it is difficult to calculate lattice parameter c, because a shoulder peak of (0 0 3) plane at 8.5° (10.2 Å) and two new peaks at 15° (5.8 Å) and 22.5° (3.9 Å) around (0 0 6) plane are gradually appeared and increased with the incorporation of vanadium species. According to the reports, the peaks at 15° (5.8 Å) and 22.5° (3.9 Å) can be ascribed to the (0 0 6) and (0 0 9) planes of Mg_2Al-$V_{10}O_{28}$-LDH [13,21]. Meanwhile, the (0 0 3) plane of Mg_2Al-$V_{10}O_{28}$-LDH is expected at 11.7 Å, however, which is covered by the broad peak at 8.5° (10.2 Å). The latter peak is thought to be due to a compound ($Mg_3V_2O_8{\cdot}14H_2O$) formed as a result of the reaction between the basic hydrotalcite and the acidic polyoxometalate or to a defect in the LDH structure resulting from acid damage [21–24]. Therefore, the new appeared three peaks further evidence the successful replacement of smaller nitrate anions by larger vanadium species $V_{10}O_{28}^{6-}$ (the size of $V_{10}O_{28}^{6-}$ is $12.8 \times 10.2 \times 7.8$ Å^3 with the cross-sectional area of 105 ± 25 Å^2) [15,25]. On the other hand, the (0 0 3) and (0 0 6) plane of Mg_2Al-NO_3-LDH were remained. However, the intensity decreases with the rise of vanadium content. Thus, the samples with different vanadium content contain a mixture of Mg_2Al-NO_3-LDH and Mg_2Al-$V_{10}O_{28}$-LDH.

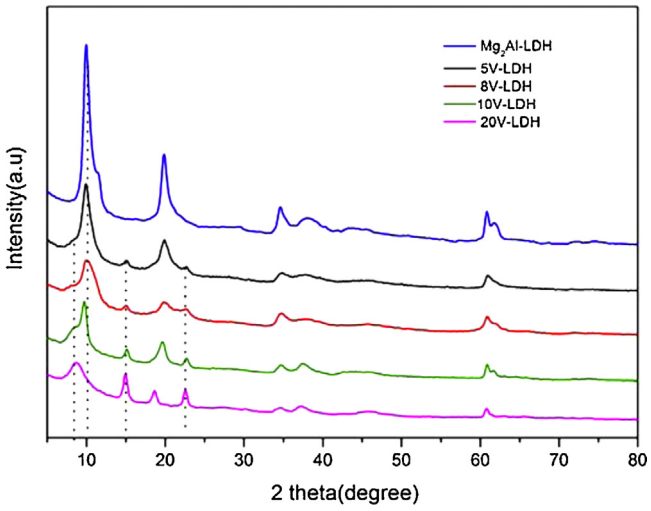

Fig. 1. XRD patterns of V-LDH.

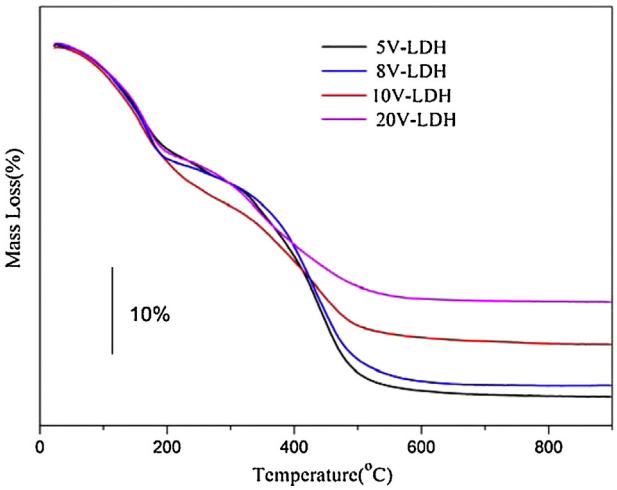

Fig. 2. TG patterns of V-LDH.

The FTIR spectra of all catalysts are shown in Fig. S1. It is known that the peak at 1380 cm^{-1} correspond to vibrations of NO_3^-. The peak intensity decreased with increasing vanadium content, indicating that the vanadium species were incorporated successfully into the interlayer. In particular, the peak is near-negligible when the vanadium content reaches 20%, suggesting the main phase existing in the interlayer is $V_{10}O_{28}^{6-}$. The peaks at 1000 cm^{-1} are related to the vibration of the M—O band. The peaks at 1620 cm^{-1} can be attributed to the bending vibration of water. Moreover, a new peak appears gradually at around 880 cm^{-1} with increasing vanadium content [26], which corresponds to vibration of the [VO_4] group. This further confirms the successful incorporation of vanadium species.

The thermal behaviors of the parent LDH materials during heating in air are illustrated in Fig. 2. Two consecutive weight loss steps were seen in all of the cases, which are typical of LDH materials [27]. The first step occurred at 100–300 °C and can be attributed to removal of interlayer water molecules [28]. The second step occurred at 300–500 °C and is probably associated with the dehydroxylation and elimination of NO_3^- [29]. The layer structure then collapses and LDH materials transform into the corresponding oxides [19,30,31]. Obviously, the weight loss in the first step is almost coincident in all cases, whereas that of the second step decreases with the rise in vanadium content. This can be interpreted as a result of more NO_3^- being replaced by $V_{10}O_{28}^{6-}$ in the anion exchange process. Thus, the thermal analysis indicated that vanadium species were incorporated into the interlayer successfully, and thermally stable phases are formed at ~550 °C (after the second weight loss and the collapse of the layer structures). Furthermore, the elemental composition of the corresponding oxides was detected by ICP-OES and XRF, respectively. The XRF analysis revealed that all of the samples contained only Mg, Al, V, and O, suggesting the total transformation of the parent LDH materials to oxides. The detailed information obtained from XRF and ICP-OES is

Table 1
Chemical analysis (ICP-OES) of prepared LDHs and derived oxides.

Sample	Mg (wt%)	Al (wt%)	V (wt%)	Mg/Al (molar ratio)
LDH	16.9	10.8	–	1.8
5V-LDH	8.9	25.0	4.9	0.4
5V-LDO	13.9	41.5	8.2	0.4
8V-LDH	11.1	23.0	7.4	0.5
8V-LDO	14.6	31.9	10.6	0.5
10V-LDH	10.3	20.8	8.6	0.5
10V-LDO	14.6	30.9	12.6	0.5
20V-LDH	8.0	17.3	13.5	0.5
20V-LDO	10.2	22.1	17.1	0.5

summarized in Table 1 and Table S1, respectively. It was observed that the XRF result is different from that of ICP-OES, which can be attributed to the fact that XRF mainly gives the bulk elemental compositon. Moreover, ICP-OES reveals that the Mg/Al of vanadium is much lower than 2, such a result could arise from a partial dissolution of Mg^{2+} during the exchange process in acidic medium (pH 4.5) [32].

Nitrogen adsorption–desorption isotherms and BJH pore size distribution, calculated from the desorption branch of all samples, are shown in Fig. 3, and the textural properties are listed in Table 2. All of the samples show type IV isotherms with clear hysteresis loops, indicating the presence of mesoporous structures [33]. Simultaneously, the step of the hysteresis loops shifts toward higher pressure with increasing vanadium content. This indicates that the pore diameter increased with the addition of vanadium

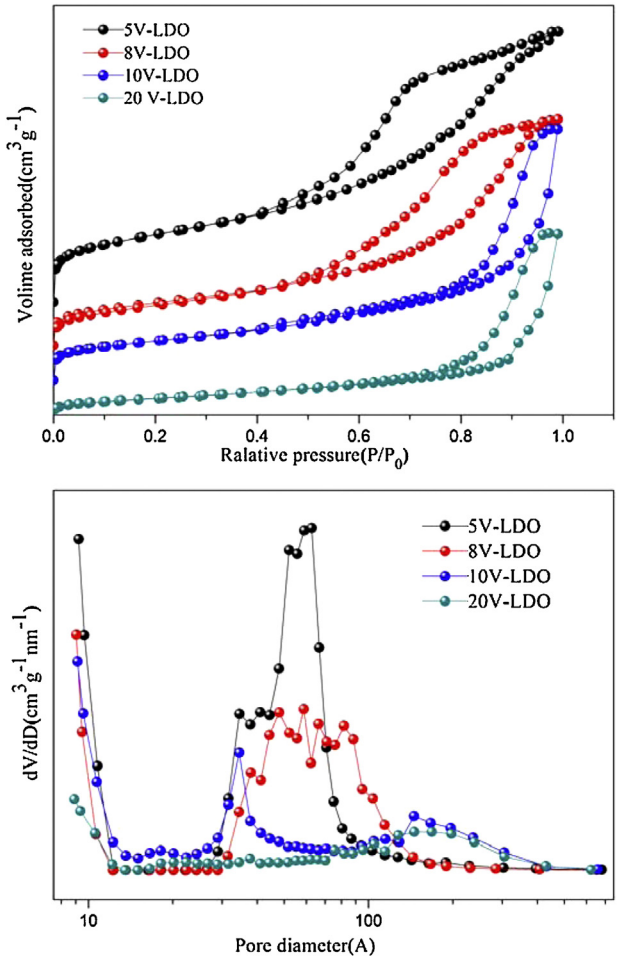

Fig. 3. Nitrogen adsorption/desorption isotherms and pore size distribution calculated from the desorption branch of V-LDO catalysts.

Table 2
Textural properties of V-LDO catalysts.

Sample	S_{BET}[a]/(m^2/g)	V_p[b](cm^3/g)	D_p[c](nm)
5V-LDO	246.8	0.42	6.7
8V-LDO	160.2	0.35	8.7
10V-LDO	142.8	0.38	10.7
20V-LDO	75.98	0.28	14.9

[a] BET specific surface area calculated at P/P_0 = 0.05–0.25.
[b] Total pore volume estimated at P/P_0 = 0.99.
[c] BJH pore diameter calculated from the desorption branch.

species [34], in accordance with the pore size distribution. Moreover, the specific surface area of all of the samples decreases with increased vanadium content. It can be deduced that larger particles, such as α-$Mg_2V_2O_7$ and $Mg_3V_2O_8$, were formed with increasing vanadium content, which is responsible for the increase in pore size and the decrease in specific surface area.

3.2. Catalytic performances of Mg_2AlVO catalysts

3.2.1. Effect of reaction temperature

Fig. 4 demonstrates the effect of reaction temperature on the catalytic performances of the LDO catalysts for H_2S selective catalytic oxidation. As shown in Fig. 4(A), the H_2S conversion initially increased with rising temperatures, up to 180 °C, and then remained almost constant when the temperature increased further to 200 °C. The variation in the trend of H_2S conversion with respect to vanadium content differed when the reaction temperature was below or exceeded 160 °C. Apparently, the 8V-LDO catalyst showed the best H_2S conversion when the temperature was below 160 °C. However, all of the catalysts showed almost the same H_2S conversion when the temperature exceeded 160 °C, with the 20V-LDO catalyst showing slightly higher H_2S conversion.

Fig. 4(B) shows the relationship between sulfur selectivity and reaction temperature. It can be seen that the sulfur selectivity was constant, at 100%, for all of the catalysts except the 20V-LDO catalyst when the temperature was ≤160 °C, and then, sulfur selectivity decreased gradually with the increase in reaction temperature and vanadium content. Sulfur selectivity decreased in the order: 8V-LDO > 5V-LDO > 10V-LDO > 20V-LDO when the temperature exceeded 160 °C. Nevertheless, sulfur selectivity was still >90% for all of the catalysts except the 20V-LDO catalyst. The 20V-LDO catalyst showed poorer sulfur selectivity, decreasing sharply from the starting temperature to 200 °C (84%).

Fig. 4(C) presents the influence of reaction temperature on sulfur yield. The figure shows a unique variation trend with respect to the rise in reaction temperature and vanadium content, because of the distinctly different variation trends of H_2S conversion and sulfur selectivity. The sulfur yield first increased with increased vanadium content, to 8V-LDO and a temperature of 160 °C, and then decreased with further increases in vanadium content and temperature. The 8V-LDO catalyst showed the highest sulfur yield at 160 °C, as high as 99%. Thus, compared to other metal oxide catalysts [3,5,35–37], the reaction temperature was effectively decreased, and catalytic activity significantly improved.

3.2.2. Effect of GHSV

The effect of GHSV on catalytic performance was evaluated with the 8V-LDO catalyst at 160 °C. As shown in Fig. 5, the sulfur selectivity was constant, at 100%, in the GHSV range of 5000–30000 h^{-1}. However, the 100% H_2S conversion only occurred when the GHSV was below 15,000 h^{-1}. Subsequently, it decreased with a further rise in GHSV, although the H_2S conversion and sulfur yield were still higher than 90%. Most metal oxides present their highest catalytic activities at higher temperature (200–300 °C) and lower GHSV (3000–10000 h^{-1}) [1,3,37,39–42]. Here, the V-LDO catalysts

Table 3
Activity comparison of different catalyst used in H_2S selective catalytic oxidation.

Reaction parameters			Temperature	Conversion	Selectivity	Yield
Catalyst	O_2/H_2S	GHSV h^{-1}	°C	%	%	%
Fe_2O_3/SiC [38]	2.5	3000	250	100	95	95
6%V_2O_5/Zr-PILC [5,37]	0.5	10000	300	98	95	93
5%V_2O_5/TiO_2-PILC [3,39]	0.5	10000	220	100	97	97
7%V_2O_5/Fe_2O_3-PILC [40,41]	0.5	10000	300	99	96	95
7%Fe/Al-Lap [2]	0.5	7000	180	98	97	95
5%V_2O_5/CeO_2-Lap [6]	0.5	7000	180	99	99	98

exhibited excellent catalytic activities at much higher GHSV and lower temperature. And the detailed comparisons of different catalysts used in H_2S selective catalytic oxidation are collected in Table 3.

3.2.3. *Durability of Mg_2AlVO catalysts*

Fig. 6 shows the durability behavior of the 8V-LDO catalyst at 160 °C with a reactant composition of $H_2S/O_2/N_2 = 5/2.5/92.5$ at GHSV = 24,000 h^{-1}. Both H_2S conversion and sulfur selectivity are almost constant, with almost no decrease after a 100 h reaction; both were as high as 97%. Because of the high and stable H_2S conversion and sulfur selectivity, the sulfur yield can also be very high, up to 95%. Thus, these results demonstrate that the Mg_2AlVO catalyst is highly durable at a relatively low temperature and a high GHSV. It can continue in a 100 h reaction with almost no deactivation. Consequently, the stability is greatly improved compared to the $Mg_2Al_xV_{1-x}O$ catalyst derived from LDH with a vanadium intercalated brucite-like layer.

To the best of our knowledge, this is the first report of a vanadium-based catalyst showing outstanding stability at a low temperature (160 °C) and a high GHSV (24,000 h^{-1}). Furthermore, it is important to explore the nature of the vanadium species present, the catalytic reaction and the deactivation mechanism, because the V-LDO catalyst exhibits excellent catalytic activities and stability at a low temperature and a high GHSV.

3.3. *Chemical status of the vanadium species in Mg_2AlVO catalysts*

The nature of the vanadium species present is important for determining the properties of the catalyst as well as the catalytic performance. The XRD patterns of the derived oxides (Fig. 7) apparently show the complete transformation from LDH to the oxide phase. In the case of 5V-LDO, 8V-LDO and 10V-LDO catalysts, similar features were observed. The patterns were dominated by peaks occurring at about 37°, 45°, and 62°, likely attributable to diffractions by planes (1 1 1), (2 0 0), and (2 2 0), respectively, of the periclase (MgO) structure [13,43,44]. However, the peaks shift toward relatively higher angles, compared to pure MgO, which is indicative of the formation of a MgO structure with defects [45]. Moreover, no peak corresponding to vanadium species was observed. This suggests that vanadium species are highly dispersed within the catalyst, and are mainly present in the form of a highly disordered amorphous phase [13]. Nevertheless, in the case of the 20V-LDO catalyst, a rather different pattern was obtained. The pattern reveals the co-existence of *a*-$Mg_2V_2O_7$ and MgO phases. This can be explained by the vanadium present in the LDH being a polymeric decavanadate species, which, on heating, partially de- and re-polymerizes and provide chains of reactive $(VO_3)_n^{n-}$ ready to form *a*-$Mg_2V_2O_7$ with its dimeric $(V_2O_7)^{4-}$ units [46].

Fig. S2 shows the FTIR spectra of the catalysts. The peaks related to NO_3^- disappeared, indicating the removal of NO_3^- species. No peak corresponding to a vanadium species is observed for 5V-LDO catalyst. However, a new peak at 960 cm^{-1} appeared gradually and was strengthened with increasing vanadium content. According to the literature [47], the peak can be attributed to the vibration of V=O and $[VO_4]$ in $Mg_2V_2O_7$. The FTIR results confirm the formation of a Mg–V mixed oxide in the process. For the 20V-LDO catalyst, an additional peak was detected at 919 cm^{-1}, attributed to $Mg_2V_2O_7$. This is in good agreement with the XRD results.

The Raman spectrum was also examined to further investigate the form of the vanadium species. As shown in Fig. S3, the spectrum characteristics differ with the increase in vanadium content. In the case of the 5V-LDO catalyst, the spectrum is dominated by a single peak appearing around 880 nm, which corresponds to the isolated tetrahedrally coordinated vanadium species: that is, $[VO_4]$. The 8V-LDO and 10V-LDO catalysts show similar features. The neat spectra reveal the presence of two bands around 880 nm, attributed to $[VO_4]$ species, and 950 nm, attributed to $Mg_2V_2O_7$ species [46,48], as the main features of the catalysts. Thus, these finding suggest that vanadium species react with Mg to form $Mg_2V_2O_7$ species with the increase in vanadium content. However, the spectrum of the 20V-LDO catalyst is dominated by four peaks at 840, 863, 905, and 950 nm. It is known that the peaks at 905 nm and 950 nm correspond to the $Mg_2V_2O_7$ species; this is in good agreement with the XRD results. Moreover, the peaks at 840 nm and 863 nm can be assigned to the presence of crystalline $Mg_3V_2O_8$ species, illustrating that partial vanadium species are present in the form of $Mg_3V_2O_8$ for the 20V-LDO catalyst. However, the absence of the peak at 880 nm indicates the disappearance of the isolated vanadium species.

In our previous work, it was observed that little vanadium existed in the V^{4+} state in the VO^{2+} form. The existence of VO^{2+} can cause a decrease in catalytic activity. Thus, the XPS method was used to further explore the vanadium chemical state. The V 2p 3/2 XPS spectra of 5V-LDO, 8V-LDO, 10V-LDO, and used 8V-LDO are shown in Fig. 8. Moreover, the catalyst elemental composition results based on XPS analysis were also presented is Table S1. It can be seen from Fig. 8 that all spectra are dominated by a broad asymmetric peak, which can be further divided into two peaks, occurring at 517.8 eV, attributable to V^{5+}, and 515.6 eV, attributable to V^{4+}. Therefore, XPS analysis reveals the co-existence of V^{5+} and V^{4+} species. For all of the samples, the spectra were dominated by the V^{5+} peak. However, the area percentages of V^{4+} peak were higher than 25%, indicating the abundant presence of V^{4+} species too. The detailed XPS results are shown in Table 4. Based on the XRD and Raman analyses, V^{5+} is primarily present in the forms of $[VO_4]$, $Mg_2V_2O_7$, and $Mg_3V_2O_8$. However, the existence form V^{4+} species

Table 4
XPS information about V-LDO catalysts.

Sample	Peak position		Area percentage	
	V^{4+}	V^{5+}	V^{4+}	V^{5+}
5V-LDO	515.65	517.85	38	62
8V-LDO	515.61	517.84	27	73
10V-LDO	515.63	517.83	35	65
Used 8V-LDO	515.97	518.01	39	61

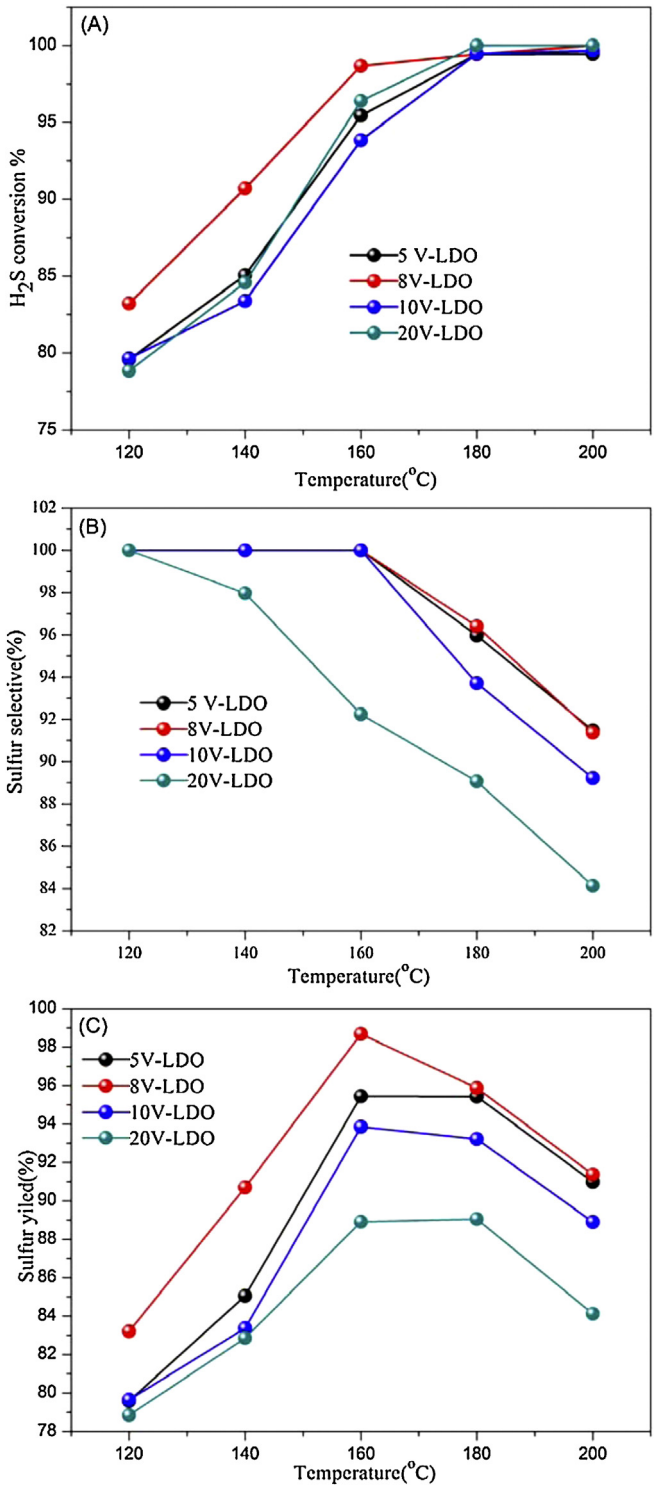

Fig. 4. Effect of temperature on (A) Conversion of H_2S, (B) sulfur selectivity and (C) sulfur yield for V-LDO catalysts.

remain unclear. Furthermore, the area percentage of V^{4+} for the used catalyst (reaction for 100 h) increased compared to the fresh catalyst, from 27% to 39%. This demonstrates that more V^{4+} species are generated during the reaction/catalytic process.

EPR was used to further explore the environment and status of the V^{4+} species in these catalysts. The EPR signals are shown in Fig. S4. It is known that the V^{5+} with a configuration d° is diamagnetic. The presence of EPR signals with a characteristic eight-line hyperfine patterns can be attributed to the interaction of the unpaired

Table 5
EPR parameters of V^{4+} present in V-LDO catalysts.

Sample	g_{II}	$g_{\perp}$	A_{II} (mT)	$A_{\perp}$ (mT)	B	$\beta_2{}^2$
5V-LDO	1.947	1.972	17.475	5.432	1.837	0.910
8V-LDO	1.956	1.967	16.591	5.432	1.300	0.852
10V-LDO	1.947	1.973	17.914	5.433	1.893	0.944
20V-LDO	1.948	1.976	17.767	5.286	2.062	0.945
Used 8V-LDO	1.946	1.980	17.936	5.140	2.480	0.966

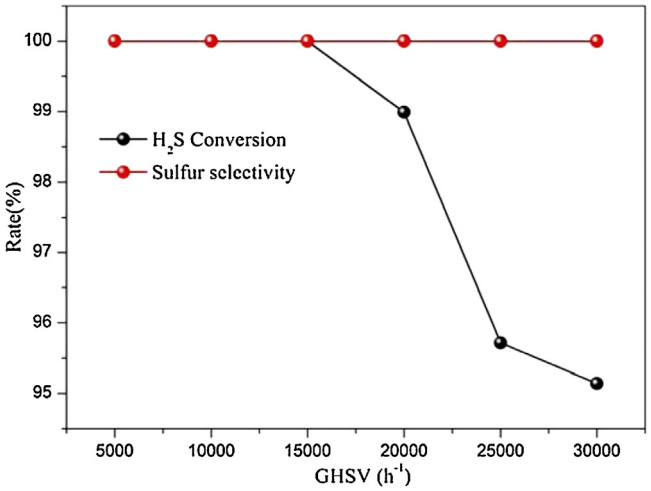

Fig. 5. Effect of GHSV on catalytic performance for 8V-LDO catalyst at 160 °C.

electron with the ^{51}V nucleus ($I = 7/2$), indicating the presence of V^{4+} species [49], which is consistent with the XPS results. Obviously, some reduction of the starting forms of vanadium occurs during the preparation process. Detailed EPR information is presented in Table 5. It is known that the values of A and g are related to the symmetry of the coordination sphere around the V^{4+} complex and to the nature of the surrounding ligands. Based on this, the experimentally observed $g_{II} < g_{\perp}$, $A_{II} > A_{\perp}$ indicates the formation of vanadyl bonds (V^{4+}) (i.e., most of the V^{4+} species are present in a form with vanadyl bonds). Significantly, more information is given by parameters B and $\beta_2{}^2$, where B is defined as $B = (g_{II} - g_e)/(g_{\perp} - g_e)$ and $\beta_2{}^2$ is defined as $\beta_2{}^2 = 7/6(g_{II} - g_e) - 5/12(g_{\perp} - g_e) - 7/6(A_{II} - A_{\perp})/P$ [50–53]. The increase in B points to either shortening of the V=O bond or to the elongation of the distance to the in-plane ligands; both can enhance the strength of the vanadyl bond [54]. The $\beta_2{}^2$

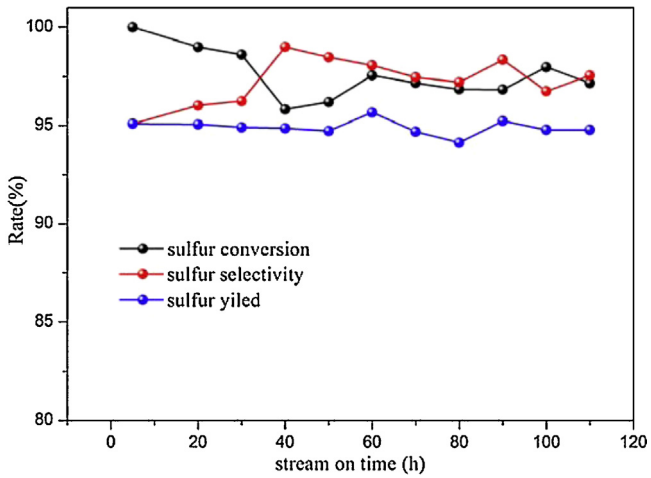

Fig. 6. Time on stream behavior of 8V-LDO catalyst for H_2S selective oxidation at 160 °C.

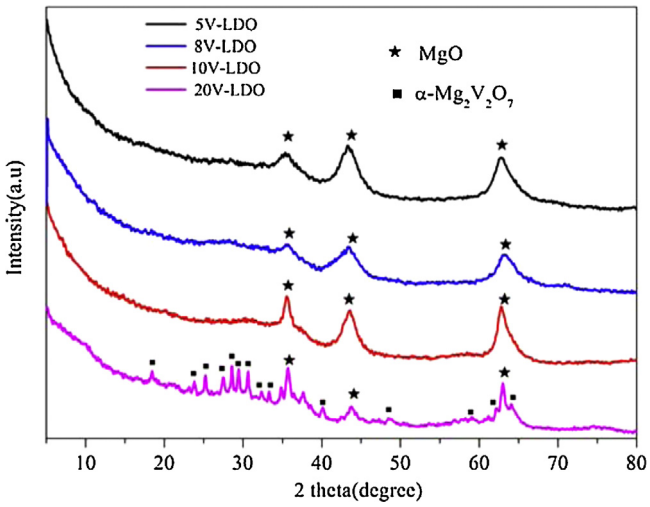

Fig. 7. XRD patterns of V-LDO catalysts.

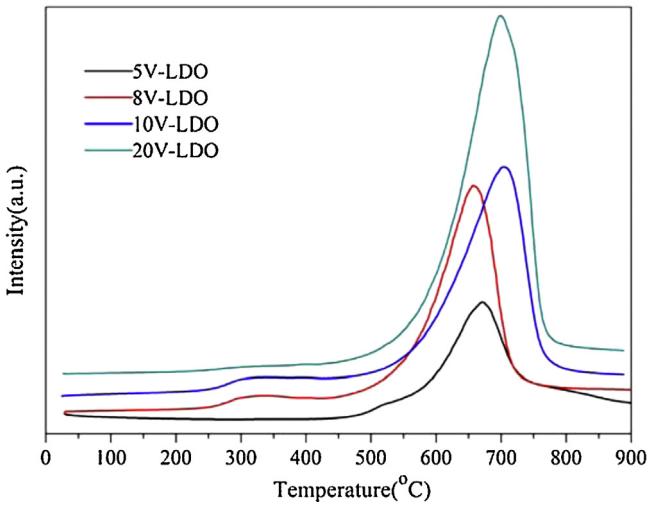

Fig. 9. H_2-TPR spectra of V-LDO catalysts.

parameter provides information about the degree of localization of the unpaired electron on the vanadium d_{xy} orbital, which in turn, informs about the extent of V—O π-covalent bonding in the plane perpendicular to the vanadyl bond. Importantly, the values of B and ${\beta_2}^2$ change with the increase in vanadium content, indicating a changing electronic structure of V^{4+}. Among them, the 8V-LDO catalyst possessed the lowest B and ${\beta_2}^2$ values, indicating the weakest vanadyl bond and a higher degree of π-covalent bonding of the V^{4+} center.

3.4. Reductive properties of Mg_2AlVO catalysts

The TPR profiles of all of the catalysts are shown in Fig. 9. All of the spectra are dominated by a single peak, centered at 600–800 °C, corresponding to the reduction of V^{5+}. However, the reduction peak shifts toward higher temperatures with an increase in vanadium content (660 °C for 5V-LDO and 8V-LDO catalysts, 700 °C for 10V-LDO and 20V-LDO catalysts). This phenomenon indicates that a lower vanadium content is favorable for redox reactions of these catalysts. In addition, all of the reduction peaks were asymmetric, indicating the presence of V^{4+} species in these catalysts too.

3.5. Catalytic mechanism of Mg_2AlVO catalysts

Our previous work revealed that vanadium-containing LDH-based catalysts obey step-wise mechanisms, and moderate basic sites (Mg—O band) in the catalyst surface play a key role in the H_2S oxidation process, where H_2S is first adsorbed on the basic sites and then reduced to elemental sulfur by vanadium species. Given this process, the basic properties of V-LDO catalysts were also assessed by CO_2-TPD; the profiles are shown in Fig. 10. Although the weak basicity is almost constant with the increase in vanadium content, the moderated basicity decreases gradually.

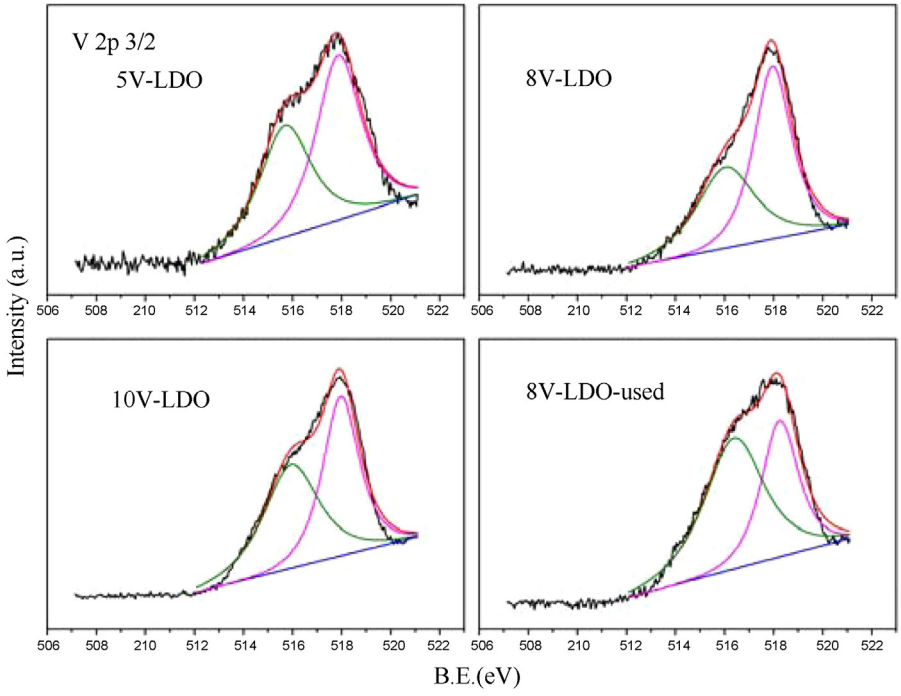

Fig. 8. V 2p3/2 XPS spectra of V-LDO catalysts.

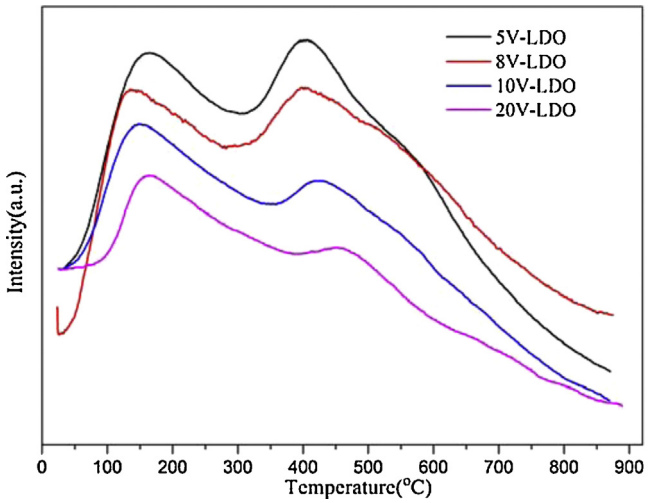

Fig. 10. CO_2-TPD spectra of V-LDO catalysts.

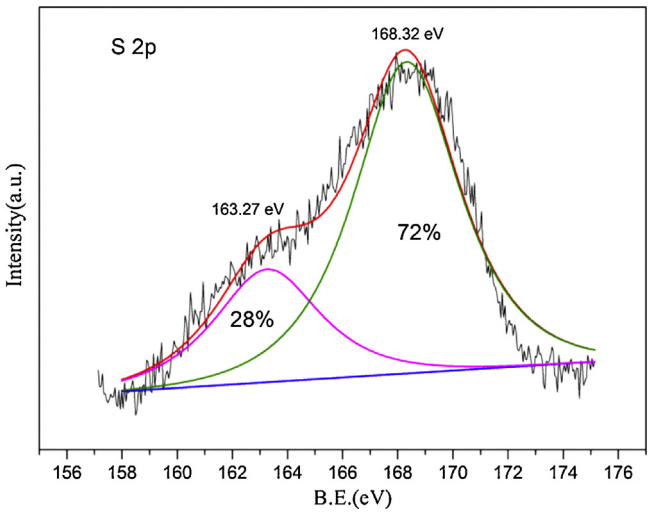

Fig. 11. S 2p XPS spectrum of used 8V-LDO catalyst.

Based on these analyses and the catalytic performances, the H_2S conversion process can be proposed tentatively and explained reasonably as follows. The active vanadium phase is not sufficiently active in the lower temperature ranges; it associates with the moderate basic site to jointly facilitate the H_2S conversion process. The H_2S conversion of the 5V-LDO catalyst depends mainly on the large number of moderate basic sites, which can abundantly adsorb H_2S. However, it is limited by the less active vanadium phase content, because it cannot effectively transform the adsorbed H_2S to elemental sulfur. Thus, the 8V-LDO catalyst showed the highest H_2S conversion below 160 °C, which is likely attributable to the appropriate amount of moderate basic sites and the active vanadium content. In addition, the improved reducibility is also favorable for the H_2S conversion. However, for the 10V-LDO and 20V-LDO catalysts, the H_2S conversions depend mainly on the amount of active vanadium phase, which can transform more adsorbed H_2S to elemental sulfur at one time. However, performance is limited by the lower content of moderate basic sites. The vanadium species are sufficiently active when the temperature was higher than 160 °C. Thus, the active vanadium species can transform the adsorbed H_2S to elemental sulfur effectively and immediately. Consequently, the catalysts display almost constant H_2S conversion when the temperature is higher than 160 °C.

As mentioned above, more V^{4+} species were present after the reaction (the used catalyst). Importantly, the EPR analysis revealed that B and ${\beta_2}^2$ increased significantly in the used catalyst. That is, the vanadyl bond (V^{4+}) was strengthened, and the degree of π-covalent bonding of the V^{4+} center was weakened after the reaction. This indicates that V^{4+} species participate in the reaction. Moreover, for fresh catalysts, both the B and ${\beta_2}^2$ increase in the order 8V-LDO < 5V-LDO < 10V-LDO < 20V-LDO. That is, the strength of the vanadyl bond decreased and the degree of π-covalent bonding of the V^{4+} center increased, in this order, consistent with the variation trend of sulfur selectivity. Thus, it can be deduced that the strength of the vanadyl bond and the degree of π-covalent bonding of the V^{4+} center influence the sulfur selectivity greatly. Likely, the stronger the vanadyl bond and the lower the degree of π-covalent nature, the easier is the reaction of oxygen and sulfur species to produce SO_2. During the reaction process, the vanadyl bond (V^{4+}) is strengthened and the degree of π-covalent bonding of V^{4+} center is weakened. Moreover, it is significantly observed that the sulfur selectivity decreased gradually with time proceed in Fig. 6, which partially evidence the above hypothesis.

Importantly, sulfur species were also detected in the used catalyst with XPS (Fig. 11). Moreover, the S-XPS signals showed two peaks, at 164 eV and 169 eV, corresponding to elemental sulfur and sulfate species, respectively. Considering that a large amount of V^{4+} existed in the catalyst and that the electronic structure of the V^{4+} species were changed after the reaction, the observed sulfate likely indicates the presence of $VOSO_4$ species in the catalyst. Moreover, the S-XPS signals were largely dominated by the latter sulfate peak. In addition, the surface sulfur content detected by XPS was 6.8 wt%; consequently, the sulfate species content was 4.9 wt% (the area percentage of sulfate species was 72%). Apparently, the molar ratio of sulfate and V^{4+} is almost 1:1, taking into account that the V^{4+} content was almost 8.19 wt% (the area percentage of V^{4+} was 39%). Thus, it can be concluded that likely all of the V^{4+} species and sulfate species in fact exist in the form of $VOSO_4$ after a reaction for 100 h (i.e., the sulfate species produced react with the vanadyl bond and the new reduced V^{4+} to form $VOSO_4$ during the reaction). Therefore, based on the above analysis, the reaction process can be tentatively proposed as follows: H_2S was first adsorbed on the moderate basic sites (Mg—O) of V-LDO catalyst and then oxidized to sulfur species (elemental sulfur and sulfate species) by V^{5+}. Meanwhile, the abundant existence of vanadyl bond (V^{4+}) was beneficial to the formation of SO_2, causing the slightly decrease of sulfur selectivity. The vanadyl bond was strengthened during the reaction process and the V^{4+} in vanadyl bond as well as partial new formed V^{4+} reacted with sulfate to form less active $VOSO_4$ species. On the other hand, the stable presence of the V^{4+} state can improve the redox property of V^{5+}, which is favorable for catalytic activity [55]. In our previous work, it was found that new VO^{2+} species was formed by occupying the Mg lattice in MgO structure, which

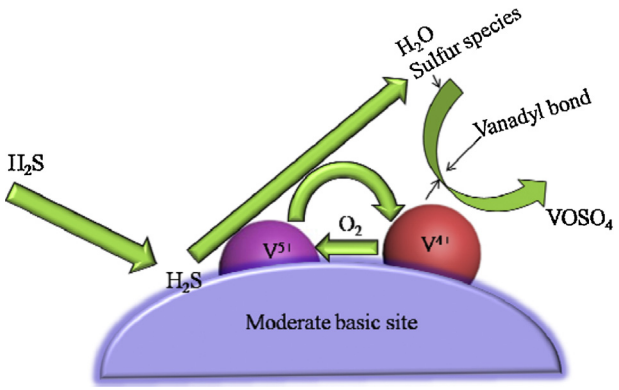

Fig. 12. Schematic of catalytic mechanism over V-LDO catalyst.

caused the decrease of MgO content. That finally caused the catalyst deactivation. However, the MgO content of V-LDO catalysts was remained consistent during the reaction. Therefore, the excellent durability of V-LDO catalysts can be ascribed to the fact that the content of moderate basic sites was kept and the redox property of V^{5+} was improved. Even though less active $VOSO_4$ species was generated and elemental sulfur deposition, which was considered as the main reason of catalyst deactivation for the other catalysts. The catalytic mechanism schematic of H_2S selective oxidation over V-LDO catalyst is shown in Fig. 12.

4. Conclusions

A series of Mg_2Al-$V_{10}O_{28}$-LDH compounds was synthesized using ion-exchange method, and the derived oxides were tested for H_2S selective oxidation. It was observed that vanadium species existed mainly in the form of isolated V^{5+} in distorted [VO_4], $Mg_3V_2O_8$, and $Mg_2V_2O_7$. Moreover, there was a large amount of V^{4+} species (>25%), existing mainly in the form of vanadyl bonded material. The strength of the vanadyl bond and the degree of π-covalent bonding of the V^{4+} center changed with increasing vanadium content and mainly related to sulfur selectivity. Significantly, the catalysts exhibited high catalytic activity at relatively low reaction temperatures (100–200 °C). Furthermore, the V-LDO catalyst showed high durability at a relatively low temperature (160 °C) and high GHSV (24,000 h^{-1}) conditions. It can be used for 100 h continuously with almost no deactivation. The catalyst obeyed a step-wise mechanism for H_2S selective catalytic oxidation. The excellent durability can be ascribed to the fact that the content of moderate basic sites was kept and the redox property of V^{5+} was improved.

Acknowledgments

This work was financially supported by the National High Technology Research and Development Program of China (No. 2012AA063101); the National Natural Science Foundation (21337003); and the Science Promotion Program of Research Center for Eco-Environmental Sciences, CAS (YSW2013B05).

The English in this document has been checked by at least two professional editors, both native speakers of English. For a certificate, please see: http://www.textcheck.com/certificate/EUhfCR.

Appendix A. Supplementary data

Supplementary data associated with this article can be found, in the online version, at http://dx.doi.org/10.1016/j.apcatb.2015.03.057.

References

[1] V.V. Shinkarev, A.M. Glushenkov, D.G. Kuvshinov, G.G. Kuvshinov, Carbon 48 (2010) 2004–2012.
[2] X. Zhang, G.Y. Dou, Z. Wang, L. Li, Y.F. Wang, H.L. Wang, Z.P. Hao, J. Hazard. Mater. 260 (2013) 104–111.
[3] K.V. Bineesh, D.-K. Kim, M.-I.L. Kim, D.-W. Park, Appl. Clay Sci. 53 (2011) 204–211.
[4] M.Y. Shin, D.W. Park, J.S. Chung, Appl. Catal. B 30 (2001) 409–419.
[5] K.V. Bineesh, D.K. Kim, D.W. Kim, H.J. Cho, D.W. Park, Energy Environ. Sci. 3 (2010) 302–310.
[6] X. Zhang, G.Y. Dou, Z. Wang, J. Cheng, H.L. Wang, C.Y. Ma, Z.P. Hao, Catal. Sci. Technol. 3 (2013) 2778–2785.
[7] A.V. Neimark, L.I. Kheifets, V.B. Fenelonov, Ind. Eng. Chem. Prod. Res. Dev. 20 (1981) 439–450.
[8] Z.P. Xu, J. Zhang, M.O. Adebajo, H. Zhang, C.H. Zhou, Appl. Clay Sci. 53 (2011) 139–150.
[9] K. Karásková, L. Obalová, K. Jirátová, F. Kovanda, Chem. Eng. J. 160 (2010) 480–487.
[10] S.H. Wang, Y.B. Wang, Y.M. Dai, J.M. Jehng, Appl. Catal. A 439–440 (2012) 135–141.
[11] C.H. Zhou, Appl. Clay Sci. 53 (2011) 87–96.
[12] X. Zhang, Z. Wang, N.L. Qiao, S.Q. Qu, Z.P. Hao, ACS Catal. 4 (2014) 1500–1510.
[13] R. Dula, K. Wcislo, J. Stoch, B. Grzybowska, E.M. Serwicka, F. Kooli, K. Bahranowski, A. Gawel, Appl. Catal. A 230 (2002) 281–291.
[14] Z.P. Xu, G. Stevenson, C.-Q. Lu, G.Q. Lu, J. Phys. Chem. B 110 (2006) 16923–16929.
[15] A.L. Maciuca, C.E. Ciocan, E. Dumitriu, F. Fajula, V. Hulea, Catal. Today 138 (2008) 33–37.
[16] J.J. Yu, Z. Jiang, L. Zhu, Z.P. Hao, Z.P. Xu, J. Phys. Chem. B 110 (2006) 4291–4300.
[17] A.N. Salak, J. Tedim, A.I. Kuznetsova, J.L. Ribeiro, L.G. Vieira, M.L. Zheludkevich, M.G.S. Ferreira, Chem. Phys. 397 (2012) 102–108.
[18] A.N. Salak, J. Tedim, A.I. Kuznetsova, M.L. Zheludkevich, M.G.S. Ferreira, Chem. Phys. Lett. 495 (2010) 73–76.
[19] F.M. Labajos, M. Dolores Sastre, R. Trujillano, V. Rives, J. Mater. Chem. 9 (1999) 1033–1039.
[20] P. Kuśtrowski, D. Sułkowska, L. Chmielarz, A. Rafalska-Łasocha, B. Dudek, R. Dziembaj, Micropor. Mesopor. Mater. 78 (2005) 11–22.
[21] J. Antonio Valverde, A. Echavarria, J.-G. Eon, A.C. Faro Jr., L. Amparo Palacio, React. Kinet. Mech. Catal. 111 (2014) 679–696.
[22] J.D. Wang, Y. Tian, R.C. Wang, A. Clearfield, Chem. Mater. 4 (1992) 1276–1282.
[23] E. Narita, P. Kaviratna, T.J. Pinnavaia, Chem. Lett. (1991) 805–808.
[24] V. Rives, M.A. Angeles Ulibarri, Coord. Chem. Rev. 181 (1999) 61–120.
[25] I. Ichinose, T. Asai, S. Yoshimura, N. Kimizuka, T. Kunitake, Chem. Lett. 23 (1994) 1837–1840.
[26] M.J. Holgado, S. San Román, P. Malet, V. Rives, Mater. Chem. Phys. 89 (2005) 49–55.
[27] P. Li, C. He, J. Cheng, C.Y. Ma, B.J. Dou, Z.P. Hao, Appl. Catal. B 101 (2011) 570–579.
[28] M.J. Holgado, F.M. Labajos, M.J.S. Montero, V. Rives, Mater. Res. Bull. 38 (2003) 1879–1891.
[29] Q.Z. Yang, D.J. Sun, C.G. Zhang, X.J. Wang, W.A. Zhao, Langmuir 19 (2003) 5570–5574.
[30] Z.P. Xu, H.C. Zeng, J. Phys. Chem. B 104 (2000) 10206–10214.
[31] P. Bera, M. Rajamathi, M.S. Hegde, P.V. Kamath, Bull. Mater. Sci. 23 (2000) 141–145.
[32] F. Kooli, I. Crespo, C. Barriga, M.A. Ulibarri, V. Rives, J. Mater. Chem. 6 (1996) 1199–1206.
[33] G.D. Wu, X.L. Wang, W. Wei, Y.H. Sun, Appl. Catal. A 377 (2010) 107–113.
[34] S.X. Xia, R.F. Nie, X.Y. Lu, L. Wang, P. Chen, Z.Y. Hou, J. Catal. 296 (2012) 1–11.
[35] K.V. Bineesh, D.K. Kim, M.I. Kim, M. Selvaraj, D.W. Park, Dalton Trans. 40 (2011) 3938–3945.
[36] J.C. Lavalley, J. Travert, T. Chevreau, J. Lamotte, O. Saur, J. Chem. Soc. Chem. Commun. (1979) 146–148.
[37] T.J. Toops, M. Crocker, Appl. Catal. B 82 (2008) 199–207.
[38] K.V. Bineesh, S.Y. Kim, B.R. Jermy, D.W. Park, J. Mol. Catal. A-Chem. 308 (2009) 150–158.
[39] P. Nguyen, D. Edouard, J.M. Nhut, M.J. Ledoux, C. Pham, C. Pham-Huu, Appl. Catal. B 76 (2007) 300–310.
[40] K.V. Bineesh, S.Y. Kim, B.R. Jermy, D.W. Park, J. Ind. Eng. Chem. 15 (2009) 207–211.
[41] K.V. Bineesh, D.K. Kim, M.I. Kim, M. Selvaraj, D.W. Park, Dalton Trans. 40 (2011) 3938–3945.
[42] K.V. Bineesh, M.-I.L. Kim, M.-S. Park, K.-Y. Lee, D.-W. Park, Catal. Today 175 (2011) 183–188.
[43] S. Blanco, S.R.G. Carrazán, V. Rives, Appl. Catal. A 342 (2008) 93–98.
[44] K. Bahranowski, G. Bueno, V. Cortés Corberán, F. Kooli, E.M. Serwicka, R.X. Valenzuela, K. Wcisło, Appl. Catal. A 185 (1999) 65–73.
[45] M.A. Ulibarri, F.M. Labajos, V. Rives, R. Trujillano, W. Kagunya, W. Jones, Inorg. Chem. 33 (1994) 2592–2599.
[46] J. Twu, P.K. Dutta, J. Catal. 124 (1990) 503–510.
[47] D. Siew Hew Sam, V. Soenen, J.C. Volta, J. Catal. 123 (1990) 417–435.
[48] J.M. López Nieto, A. Dejoz, M.I. Vazquez, W. O'Leary, J. Cunningham, Catal. Today 40 (1998) 215–228.
[49] K. Bahranowski, R. Dula, F. Kooli, E.M. Serwicka, Colloids Surf. A 158 (1999) 129–136.
[50] D. Kivelson, S.K. Lee, J. Chem. Phys. 41 (1964) 1896–1903.
[51] K. DeArmond, B.B. Garrett, H.S. Gutowsky, J. Chem. Phys. 42 (1965) 1019–1025.
[52] B.R. McGarvey, J. Chem. Phys. 71 (1967) 51–66.
[53] J.R. Morton, K.F. Preston, J. Magn. Reson. (1969) 30 (1978) 577–582.
[54] V.K. Sharma, A. Wokaun, A. Baiker, J. Chem. Phys. 90 (1986) 2715–2718.
[55] M.D. Soriano, J.M. López Nieto, F. Ivars, P. Concepción, E. Rodríguez-Castellón, Catal. Today 192 (2012) 28–35.